



5G passive optical network employing all optical-OFDM_Hybrid SSMF/FSO

Ibrahim Luay¹ · Tahreer Safa'a Mansour¹ · Somia A. Abd El-Mottaleb²

Received: 1 October 2023 / Accepted: 13 February 2024 / Published online: 8 April 2024
© The Author(s), under exclusive licence to Springer Science+Business Media, LLC, part of Springer Nature 2024

Abstract

In this paper, a new 5G Passive Optical Network (5G-PON) employing all-optical orthogonal frequency division multiplexing (AO-OFDM) is proposed in hybrid bidirectional standard single mode fiber (SSMF)/free space optical (FSO). Additionally, an optical frequency generator (OFG) source is utilized. The proposed model is simulated using VPI photonics software. Analytical modeling and simulations have been conducted for a new approach to generate OFG by cascaded two-frequency modulators and one electro-absorption modulator. A sinusoidal RF signal source is utilized to drive all these modulators. The results reveal that 64 optical multiplexed carriers with a frequency spacing of 30 GHz are generated. These optical carriers have power variations of < 1 dB. Moreover, the center wavelength of the generated OFG can be tuned from 1300 nm for upstream transmission to 1577 nm for downstream transmission in the proposed 5G-PON. The proposed network achieves 960 Gbps and 10 Gbps for the downstream and upstream directions, respectively, under different turbulence effects. Furthermore, when 32 AO-OFDM channels are used, the simulation results show that the proposed model can achieve a SSMF length and FSO propagation ranges of 20 km and 2 km, respectively, with bit error rate (BER) ($< 10^{-3}$).

Keywords 5G · PON · AO-OFDM · OFG · OLT · FSO · ONU · OMCs

1 Introduction

Currently, researchers are defining 5G, as the next generation of wireless communication. The most significant announcements on future 5G include introducing new communications technology, enhancing network capacity and speed, and emphasizing tiny cell

✉ Ibrahim Luay
ibrahim.jabar0901@ilps.uobaghdad.edu.iq

Tahreer Safa'a Mansour
tahreer@ilps.uobaghdad.edu.iq

Somia A. Abd El-Mottaleb
somaya8839@gmail.com

¹ Institute of Laser for Postgraduate Studies, University of Baghdad, Baghdad, Iraq

² Alexandria Higher Institute of Engineering and Technology, Alexandria, Egypt

concepts (Andrews et al. 2014). To enable communication for possibly billions of wireless devices, speed and capacity improvements are needed. A substantial bandwidth is available for millimeter wave bands (30–300 GHz) wireless access networks (WANs), providing an alternative for 5G applications requiring high-speed indoor/hotspot connectivity. In order to facilitate the integration of millimeter-wave radio and tiny cells for 5G access in the future, fiber-optic communication, or passive optical networks PONs is crucial for both fronthaul and backhaul networks. Fiber optic connections are made between all WAN kinds to provide an end-to-end transport network. Fiber to the x (FTTX) applications can access extremely fast Internet through optical access networks (OAN) via optical line terminals (OLT). On the other side, small-cell and mm-wave WAN are employed, which are convenient and fast. A number of bands, including the license-free band at 60 GHz, the E-band at 71–76 GHz, 81–86 GHz, and 92–95 GHz, and the local multipoint distribution service at 28–30 GHz, are now accessible for 5G high-speed wide area networks (Boccardi et al. 2014; Osseiran et al. 2014; Fadzlina Naim et al. 2021; Chang et al. 2013). Therefore, PON and WAN appear to be the most viable options for providing end consumers cost-effective last-mile access to high-speed data. PON, which uses AO-OFDM, is a superb option for a broadband access network in the future since it can give each end node with almost infinite bandwidth and higher capacity access (Fady El-Nahal et al. 2023; Hammadi and Mansour 2019). The OFDM subcarriers of AO-OFDM systems are produced optically, and optical components are used to optically implement IFFT/FFT processing. Compared to traditional OFDM subcarriers, each subcarrier has a high data information rate and is modulated by an external modulator. Consequently, AO-OFDM systems can achieve both a high data rate and a large transmission capacity (Martín-Mateos et al. 2017). An OFG source is used to show the all-optical OFDM system (Li et al. 2014; Hammadi and Mansour 2019). Due to geographical restrictions, the PON system might not be the ideal choice in places where installing fiber is expensive and difficult. Therefore, it can be combined with FSO technology to solve this issue (Yeh et al. 2019, 2020; Li et al. 2018). The benefits of FSO communication system include immunity to interference from electromagnetic waves, low power consumption, high-speed data transmission, urban implementation, license-free spectrum, and huge bandwidth (Kantarci and Mouftah 2012; Sharma and Malhotra 2022; El-Mottaleb et al. 2022). Due to these benefits, FSO communication is utilized in aircraft, maritime, internet-of-things (IoT) that serve end users, terrestrial transmission, and radio frequency RF connection backup. However, atmospheric turbulence brought on by temperature changes is the main element that deteriorates the performance of the optical signal during its propagation in the FSO channel (Mirza et al. 2020a, b). Furthermore, FSO systems frequently employ point-to-point (P2P) or point-to-multi-point (P2MP) connections. Wavelength division multiplexing (WDM) technology, which offers a high fan-out (i.e., a substantial number of channels per FSO connection) and elastic topologies, can be used to create high-capacity FSO connections (Hamza et al. 2019). Since each link needs a separate pair of telescopes, there is no capacity concern. Furthermore, FSO systems are deployed and used for fiber backup connectivity and last-mile access in P2P to guarantee network security and get beyond geographic constraints (Yeh et al. 2019). To accommodate the constantly rising traffic demand, mobile network operators are thinking about substantially adding more tiny cells to their networks in order to increase network capacity. This small-cell strategy has emerged as the most often-used method for network growth. Fronthaul communication between the Base Band Unit (BBU) and Radio Remote Head (RRH) is typically provided by wireless choices like millimeter wavelengths, microwaves, or fiber-optic networks, or wired solutions such optical fiber-based network. With its low latency, affordability, and ease of use, WDM-PON is a great option for 5 G Mobile

Front Haul (MFH) applications. A WDM-PON with a speed of 25 Gbps or more and a dedicated wavelength for every user has been proposed for 5 G deployment (Shbair and El-Nahal 2021; Luay and Mansour 2023). Because fiber deployment is not always feasible or affordable, the construction and upkeep of a stand-alone PON system may not be feasible for the deployment of fronthaul/backhaul networks, particularly in densely populated areas. To lower the fronthaul network's cost, PON and FSO can be combined. FSO fronthaul links provide for a significant reduction in deployment costs by providing a more affordable option than fiber-based fronthaul (Jaffer et al. 2021). The expensive cost of each component in WDM-PON systems has prevented their widespread deployment. Due to the widespread application of WDM-PON in long-haul and urban transmissions, no standards have been established yet. Thus, 5G PON-based AO-OFDM employing OFG is a strong candidate for next-generation access (NGA) networks in the upcoming years due to its higher performance over existing WDM-PON systems and ability to provide a long-term alternative.

Although the AO-OFDM-based radio over FSO (Ro-FSO) technology has advanced recently for both indoor and outdoor applications, the majority of these works have addressed implementation-related concerns rather than expanding the total amount of services available in the Ro-FSO system (Ahmed et al. 2015). Since Ro-FSO essentially consists of analogue transmission connections, obtaining adequately robust and dependable signals is a key issue. Creating extra optical carriers, or OFG, in the transmitter part is one way to potentially improve the number of channel services. Narrow channel spacing multi-carrier optical sources have been developed to satisfy the needs of dense WDM and super dense WDM networks. Numerous approaches have been put out to create compact multi-carrier optical sources at a reasonable cost that can supply all the channels needed to meet optical communication standards. The supercontinuum (SC) generation is the foundation of these designs (Mori et al. 2001).

In this work and to the best of our knowledge, we will combine one electro-absorption EAM and two cascaded FMs with a polarization beam splitter (PBS) in hybrid 5G bidirectional PON-FSO for the first time to increase the transmission capacity. The main contributions are:

- Proposing a new approach for producing OFG using EAM and a cascade of two FMs.
- Investigating the effect of frequency deviation for FM, as it is a significant contributing element to the rise in OMCs.
- Studying the effect of atmospheric turbulence, which is a major factor that causes degradation to the FSO link.
- Evaluating the performance of the suggested PON model based on AO-OFDM by using OFG to use its in 5G applications.

In this paper, we investigated a hybrid bidirectional PON-FSO architecture for 5 G fronthaul that uses AO-OFDM based on OFG and allows fiber to be deployed wherever it is practical and affordable. Then, in order to increase this access to several sites and ultimately connect mobile users, FSO linkages would be used. Since multi-optical sources are not required for downstream/upstream transmission, the OFG method is used here to save costs and enhance transmission capacity. Here, 960 Gbps and 10 Gbps OOK AO-OFDM signals can be transmitted over a 20 km SSMF and 2 km FSO link for downstream and upstream traffic, respectively. The proposed 5G-PON hybrid bidirectional SSMF-FSO network offers mobility, faster deployment timelines, and low-cost high-data-rate signal transmission.

The rest of the paper is arranged as follows. A basic explanation of OFG and 5G-PON is provided in Sects. 2 and 3, respectively. The simulation results and discussions are presented in Sect. 4, followed by the main conclusion in Sect. 5.

2 Construction of optical frequency generator and analytical modelling

Figure 1 shows the arrangement of the OFG source employing two FMs in cascade and one EAM. To generate (RF) signals, this configuration includes a function generator, two FM modulators, an EAM, and a continuous wave (CW) laser. The CW laser module simulates a distributed feedback (DFB) laser that generates an optical signal. While all the modulators are driven by the same frequency RF signal, emit light through the cascaded FMs-EAM. The CW laser is launched to the FM, a DFB device that modulates the phase of the optical signal through the electric field, in order to create OMCs from OFG. An optical phase modulator is monolithically integrated into a semiconductor amplifier, and optical frequency modulation can be produced using a widely tunable sampled-grating distributed Bragg reflector laser (Johansson et al. 2004). The FM 1 modulates the CW laser first, followed by the FM 2 modulation, to produce OMCs. By applying an electric voltage, EAM modifies the strength of the modulated FM 2 signal and produces OMCs at the output.

The FM’s transfer function is expressed as (Gao et al. 2016):

$$H_{FM}(t) = e^{jn_{fm} \cos 2\pi f_o t} \tag{1}$$

where f_o is the frequency of the RF signal, n_{fm} is the modulation index of FM. The Jacobi–Anger theorem allows for the expansion of Eq. (1) as:

$$H_{FM}(t) = \sum_{i=-\infty}^{\infty} J_i(n_{fm}) e^{i2\pi i f_o t} \tag{2}$$

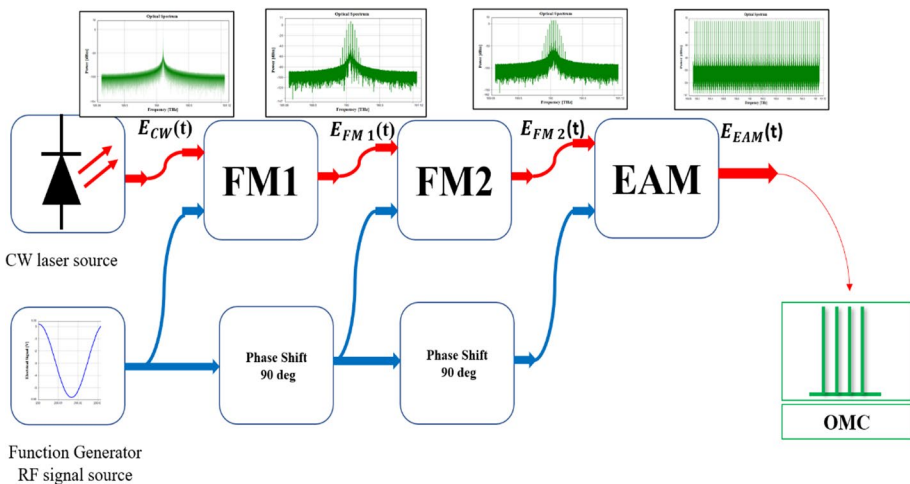


Fig. 1 Schematic diagram for the OFG source composed of two FMs and one EAM to produce OMCs

where $J_i(\cdot)$ denotes the i^{th} order of the Bessel function of the first kind. The CW light is produced by the laser source using an electric field $E_{CW}(t)$ is expressed as:

$$E_{CW}(t) = \sqrt{P_{inc}} e^{j2\pi f_c t} \tag{3}$$

where P_{inc} and f_c represent the CW laser’s power and center frequency, respectively.

An RF signal at FM 1 with a frequency of f_o modulates the CW laser, producing multiple optical carriers with a f_o frequency spacing. The signal that generates the FM 1’s output can be expressed as:

$$\begin{aligned} E_{FM1}(t) &= E_{CW}(t)H_{FM}(t) = \sqrt{P_{inc}} \sum_{i=-\infty}^{\infty} J_i(n_{fm}) e^{j2\pi(f_c + if_o)t} \\ &= \sqrt{P_{inc}} \{ J_0(n_{fm}) e^{j2\pi f_c t} + J_1(n_{fm}) e^{j2\pi(f_c + f_o)t} \\ &\quad + J_{-1}(n_{fm}) e^{j2\pi(f_c - f_o)t} + J_2(n_{fm}) e^{j2\pi(f_c + 2f_o)t} \\ &\quad + J_{-2}(n_{fm}) e^{j2\pi(f_c - 2f_o)t} + \dots \} \end{aligned} \tag{4}$$

Analyzing Eq. (4) demonstrates the following information:

- The CW laser’s center frequency determines the OFG source’s center frequency line. Thus, by adjusting the CW laser’s center frequency, the center frequency of the produced OFG can be adjusted.
- The RF signal frequency f_o is directly correlated with the frequency separation between OMCs. As a result, the OFG source may produce OMCs in a broad range of the RF driving signal’s frequency, making it simple to adjust the OMCs’ frequency spacing.
- The modulation index of the modulator is directly correlated with the number of OMCs.

According to Eq. (4), additional OMCs with the best spectral flatness can be produced by raising the modulation index. A number of modulators are cascaded together in order to raise the modulation index. Additionally, to increase the number of OMCs, the EAM is related to two FMs in the suggested OFG source. Hence, the EAM’s transfer function is expressed as (Gao et al. 2016; Ujjwal and Thangaraj 2018; Hammadi et al. 2022).

$$\begin{aligned} H_{EAM}(t) &= \sum_{k=1}^{\infty} \sum_{n=1}^{\infty} \left\{ \frac{U_b^{(2n-1)}}{(2n-1)!} C_{(2k-1)(2n-1)} \frac{A^{2n-1}}{4^{n-1}} \cos[(2k-1)2\pi f_0 t] \right. \\ &\quad \left. + \frac{U_b^{(2n)}}{(2n)!} C_{(2k)(2n)} \frac{A^{2n}}{2^{2n-1}} \cos[(2k)2\pi f_0 t] \right\} \end{aligned} \tag{5}$$

By using Euler’s formula, Eq. (5) can be written as:

$$\begin{aligned} H_{EAM}(t) &= \frac{1}{2} \sum_{k=1}^{\infty} \sum_{n=1}^{\infty} \left\{ \frac{U_b^{(2n-1)}}{(2n-1)!} C_{(2k-1)(2n-1)} \frac{A^{2n-1}}{4^{n-1}} (e^{j(2k-1)2\pi f_0 t} + e^{-j(2k-1)2\pi f_0 t}) \right. \\ &\quad \left. + \frac{U_b^{(2n)}}{(2n)!} C_{(2k)(2n)} \frac{A^{2n}}{2^{2n-1}} (e^{j4\pi k f_0 t} + e^{-j4\pi k f_0 t}) \right\} \end{aligned} \tag{6}$$

where $U_b^{(\cdot)}$ is the series coefficients of the DC component, A is the amplitude of the RF signal, and C_{kn} is a series factor related to the amplitude of the RF signal.

At the EAM's output, the created OFG is stated as:

$$\begin{aligned}
 E_{EAM}(t) &= E_{FM1}(t)H_{EAM}(t) = \frac{1}{2} \sqrt{P_{inc}} \sum_{i=-\infty}^{\infty} \sum_{k=1}^{\infty} \sum_{n=1}^{\infty} J_i(n_{fm}) e^{j2\pi(f_c + if_o)t} \\
 &\left\{ \frac{U_b^{(2n-1)}}{(2n-1)!} C_{(2k-1)(2n-1)} \frac{A^{2n-1}}{4^{n-1}} (e^{j(2k-1)2\pi f_0 t} + e^{-j(2k-1)2\pi f_0 t}) \right. \\
 &\quad \left. + \frac{U_b^{(2n)}}{(2n)!} C_{(2k)(2n)} \frac{A^{2n}}{2^{2n-1}} (e^{j4\pi k f_0 t} + e^{-j4\pi k f_0 t}) \right\} = \frac{1}{2} e^{j2\pi f_c t} \sqrt{P_{inc}} \sum_{i=-\infty}^{\infty} \sum_{k=1}^{\infty} \sum_{n=1}^{\infty} J_i(n_{fm}) \quad (7) \\
 &\left\{ \frac{U_b^{(2n-1)}}{(2n-1)!} C_{(2k-1)(2n-1)} \frac{A^{2n-2}}{4^{n-1}} [e^{j2\pi(2k+i-1)f_0 t} + e^{-j2\pi(2k-i-1)f_0 t}] \right. \\
 &\quad \left. + \frac{U_b^{(2n)}}{(2n)!} C_{(2k)(2n)} \frac{A^{2n}}{2^{2n-1}} [e^{j2\pi(2k+i)f_0 t} + e^{-j2\pi(2k-i)f_0 t}] \right\}
 \end{aligned}$$

The number of OMCs produced by the EAM is dictated by U_b and A , as can be seen from Eq. (7). Given that U_b is constant, A thus controls the number of OMCs. Additionally, the RF signal's frequency controls the frequency interval between the OMCs. When it comes to the proposed 5G PON-based all optical orthogonal frequency division multiplexing (AO-OFDM) network, OMCs can serve as subcarriers.

3 Proposed 5G PON based on AO-OFDM

The performance of the proposed optical communication network 5G PON based AO-OFDM with the intended OFG source is discussed in this section. In both upstream and downstream directions, the 5G PON hybrid SSMF / FSO consists of an optical network unit (ONU), an optical distribution network (ODN), an optical line termination (OLT), and the central office (CO). In the proposed network, OMCs are provided by the CO through

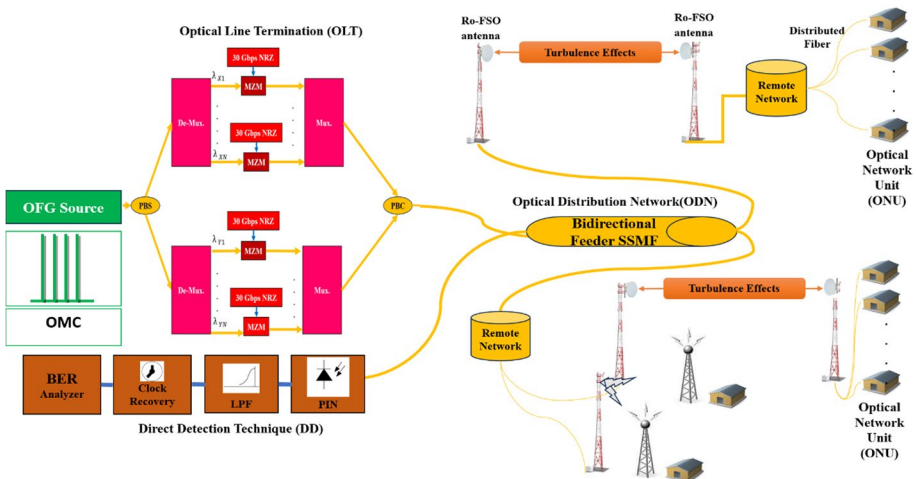


Fig. 2 Schematic diagram of 5G PON-based AO-OFDM hybrid SSMF/FSO

the OFG source. Orthogonal subcarriers are optically provided by the OFG source, which is utilized as an OMC. The independent modulation of these subcarriers precedes their combination to generate the AO-OFDM signal. If optical carriers are given precise optical frequency control, the orthogonality of the optical OFDM signal can be maintained. To satisfy the orthogonality criteria, the frequency separation between two consecutive optical orthogonal carriers is modified to equal the symbol rate. Moreover, to reduce crosstalk between optical orthogonal subcarriers, a phase correlation, is necessary between each optical subcarrier. The OMCs are used in 5G PON based AO-OFDM hybrid SSMF/FSO to achieve these conditions. A set of optical orthogonal carriers with a specified frequency spacing and phase can be produced by the OFG source. All the subcarriers have an intrinsic phase correlation since optical orthogonal subcarriers are produced by a single laser source. Figure 2 shows how the 5G PON hybrid SSMF/FSO is configured that is simulated using VPI software. As seen in Fig. 2, the components of the OLT transmitter subsystem are an OFG source, an optical de-multiplexer (De-Mux), the rotational polarization, Mach Zehnder (MZ) modulators, an optical multiplexer (Mux), and the polarization beam combiner (PBC). Section II illustrates how the OFG source portion uses cascaded FMs-EAM that is directly driven by a sinusoidal RF signal.

Because distinct subcarriers must be created from the same laser source in order to have sufficient coherence and maintain the orthogonality among the AO-OFDM subcarriers, optical orthogonal carriers are crucial for 5G PON hybrid SSMF/FSO. The fork module splits the optical orthogonal carriers that an OFG source generates into two polarization (X and Y) states. The rotation of the polarization causes the Y state to spin 90 degrees. The optical De-MUX divides these pathways, which are then applied concurrently to external optical modulators. Each of these subcarriers is modulated separately utilizing MZ modulators.

A non-return-to-zero (NRZ) line code is used to encode the 30 Gbps data signal from the pseudo random bit sequence (PRBS) generator. The MZ modulator then modulates this signal on optical orthogonal carriers to create the AO-OFDM signal. Next, the polarization combiner and MUX combine the modulated data orthogonal carriers before sending them to the transmission network.

The AO-OFDM symbol duration is set to $T_0 = \frac{1}{\Delta f_0}$ where Δf_0 is the frequency-spacing between optical orthogonal multicarrier, as illustrated in Fig. 3, in order to maintain the orthogonality of the AO-OFDM signals. Additionally, there is no need for a guard interval.

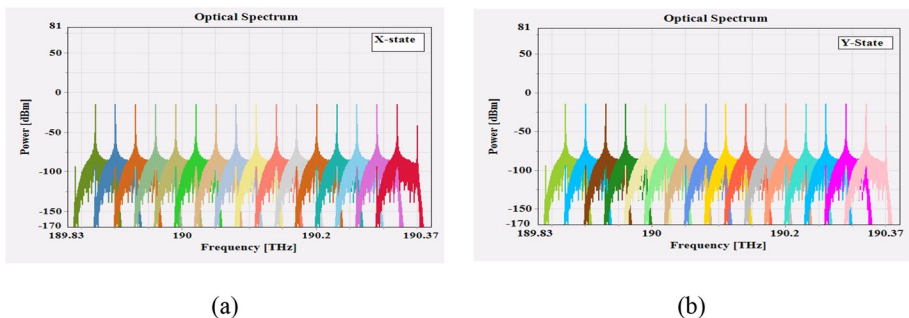


Fig. 3 Optical spectrum of AO-OFDM signals using OFG source and the optical demultiplexer at **a** X-direction and **b** Y-direction

It is observed from Fig. 2, that the OLT receiver portion uses a straightforward direct detection (DD) technique to detect the upstream signal.

The bidirectional SSMF, FSO channel, PBC, the optical De-MUX, and the remote network, represented by PBS, make up the optical distribution network (ODN). The first option for an optical link is to use the feeder SSMF or FSO channel. The optical link, as depicted in Fig. 2, also makes use of cascaded bidirectional feeder fiber SSMF and FSO. A direct connection between the radio over FSO (Ro-FSO) antenna and the bidirectional SSMF is possible if the ONU was dispersed in a single area. In contrast, the distant network established a direct downstream connection with the bidirectional SSMF even if the ONUs were dispersed among different locations. The polarization beam splitter, which divides the incoming signal from ODN into X and Y states, and the De-MUX, which demultiplexes X and Y states so that each may be independently detected using a straightforward DD technique, make up the user termination (ONU receiver) in the downstream direction. Direct modulation laser (DML) in the upstream direction, with DFB acting as an optical carrier, makes up the ONU transmitter. Each channel's 10 Gbps data stream from the PRBS generator is directly modulated by a DFB laser before being transmitted via ODN. First, from the proposed 5G PON design, the OMCs with 30 GHz frequency spacing between each frequency are generated utilizing the proposed OFG source. Subsequently, we employed the AO-OFDM signal to be sent in a 5G small cell in order to exploit the created OMCs in 5G applications. As seen in Fig. 3, the AO-OFDM signal is produced for this purpose by employing an OFG source that is demultiplexed by De-MUX. Following the modulation of a subset of OMCs, bidirectional SSMF was used to multiplex and transmit the modulated and unmodulated carriers to the Ro-FSO antenna. The optical wireless signal was coupled into SSMF at both ends of Ro-FSO antennas using collimators using the specifications for the Ro-FSO channel listed in Table 1. These Ro-FSO antennas used an optical circulator, boost and post amplifiers, and independent transmit and receive signals.

Furthermore, atmospheric attenuation and intensity scintillation have a major influence on the FSO channel (Mirza et al. 2019). The turbulence of an optical signal is estimated using a variety of FSO statistical channel models, such as the Log-normal model, K model, Negative exponential model, Gamma-Gamma model, and Log-normal Rician model (Mirza et al. 2020a, b; Kaushal et al. 2017; Luong et al. 2013; Feng and Zhao et al. 2017a, b). Log-normal model is used for WT and CA weather conditions (Kaushal et al. 2017), while for ST, K-distribution model is used (Luong et al. 2013). The commonly used model that is suitable for

Table 1 Specifications of the Ro-FSO link (Abul El-Mottaleb et al. 2023; Mehtab Singh et al. 2023)

Parameters	Values
Atmospheric turbulences considered	Weak turbulence (WT), moderate turbulence (MT) and Strong turbulence (ST)
Turbulence model	Gamma–gamma distribution
Transmitter aperture diameter	2 cm
Receiver aperture diameter	10 cm
L_{FSO}	2 km
Type of PD	PIN
Responsivity of the PD	0.85 A/W
Thermal noise power density	10^{-11} W/Hz

different turbulences (WT, MT, and ST) is gamma-gamma distribution, so it is considered in this paper (Jaffer et al. 2021; Feng and Zhao 2017a, b). The normalized light intensity I 's probability density function in this instance is provided by (Feng and Zhao 2017a, 2018; b; Lin and Sharma 2022; Elsayed et al. 2022):

$$P(I) = \frac{2(\alpha\beta)^{\frac{\alpha+\beta}{2}}}{\Gamma(\alpha)\Gamma(\beta)} \left(\frac{I}{\langle I \rangle}\right)^{\left(\frac{\alpha+\beta}{2}\right)-1} K_{\alpha-\beta} \left(2\sqrt{\alpha\beta\left(\frac{I}{\langle I \rangle}\right)}\right) \tag{8}$$

$$\alpha = \left\{ \exp \left[\frac{0.49\sigma_l^2}{\left(1 + 1.11\sigma_l^{12/5}\right)^{7/6}} \right] - 1 \right\}^{-1} \tag{9}$$

$$\beta = \left\{ \exp \left[\frac{0.51\sigma_l^2}{\left(1 + 0.69\sigma_l^{12/5}\right)^{5/6}} \right] - 1 \right\}^{-1} \tag{10}$$

where Γ is the gamma function and K_n is the modified Bessel function of the second kind of order n . α and β are the gamma-gamma distribution parameters describing the effects of large-scale and small-scale scintillation, respectively and σ_l^2 is the Rytov variance which differs according to the value of the refractive index, C_n^2 and is expressed as (Vetelino et al. 2007; Yousif et al. 2019; Elsayed and Yousif 2018; Elsayed and Yousif 2020a, b, c, d):

$$\sigma_l^2 = 1.23C_n^2K^{7/6}L_{FSO}^{11/6} \tag{11}$$

where K is the wave number and equal to $\left(\frac{2\pi}{\lambda}\right)$. The values of C_n^2 for WT, MT, and ST, are $1 \times 10^{-17} m^{-2/3}$, $5 \times 10^{-15} m^{-2/3}$, and $1 \times 10^{-13} m^{-2/3}$, respectively. Moreover, the different FSO propagation ranges can be distinguished by the σ_l^2 , as if $\sigma_l^2 < 1$, then that means WT occurs, while if $\sigma_l^2 \sim 1$, then MT occurs, and if $\sigma_l^2 > 1$, so there is ST and if σ_l^2 goes to infinity then that means that turbulence is saturated. In this study, the network performance under external atmospheric conditions WT, MT, and ST are considered. The performance of the proposed PON is evaluated using BER, eye diagrams, the average received optical power, and the pointing error. The ratio of signal to noise (SNR) can be stated as (Chaudhary et al. 2020; Abd El-Mottaleb et al. 2022; Elsayed and Yousif 2020a, b, c, d):

$$SNR = \frac{(I_{ph})^2}{\sigma_{Sh}^2 + \sigma_{th}^2} \tag{12}$$

where I_{ph} is the photocurrent, σ_{Sh}^2 is the shot noise and equals to $(2ev\mathcal{R} \langle I_{ph} \rangle)$, (e is the charge of the electron and v is the electrical bandwidth) and σ_{th}^2 refers to the thermal noise and equals to $\left(\frac{4k_B T v}{R_L}\right)$, (k_B is the Boltzman constant, T is the absolute temperature of receiver, and R_L is the load resistance. Finally, the BER is given as (Jarangal et al. 2022).

$$BER = \frac{1}{2} \operatorname{erfc} \left(\frac{\sqrt{SNR}}{2\sqrt{2}} \right) \tag{13}$$

Table 2 Specifications of the proposed Network design (Gao et al. 2016; Ujjwal and Jaisingh Thangaraj 2018; Guang Li et al. 2019)

Parameters	Values
Symbol rate	30 GHz
Channel spacing between OMCs	30 GHz
Bit per symbol	2
Number of channels	32 (16 X-state, 16 Y-state)
The data rate for each individual OLT	30 Gbps
Sample Rate	64* symbol rate
Sample mode center frequency	190.1 THz
Sample mode Bandwidth	12,800 GHz
Time window	1024/symbol rate*4
Modulation index for EAM	0.99
Length of standard single-mode fiber (SSMF)	20 km
Attenuation	0.2 dB/km
Frequency offset between modulated marks and spaces for FM	10 GHz
The output power of the modulated signal 1	5 dBm
Amplitude of RF signal	3 V
Frequency of RF signal	30 GHz
Phase of RF signal	90°
DC offset of RF signal	-2.8
Output data type	Block mode
Amplifier type	Gain controlled
Number of channels within the spectral flatness of 1 dB spectral flatness	64 Less than 1 dB
The output power of OFG signals	0 dBm
Optical orthogonal carriers	(189.9, 189.93, 189.96, 189.99, 190.02, 190.05, 190.08, 190.11, 190.14, 190.17, 190.2, 190.23, 190.26, 190.29, 190.32 and 190.35) THz
Reference frequency	190.11 THz
The rotation angle of the xy-coordinate system (polarization axes)	90°
Emission frequency of CW laser (downstream transmission)	190.1 THz
Average power of CW laser	5 dBm
Linewidth of CW laser	1 MHz
Emission frequency of DFB laser (upstream transmission)	230.6 THz
Insertion loss of modulators	5 dB

where $erfc$ refers to the error complementary function. Table 2 shows the values for the parameters used in simulation the proposed 5G PON based OFDM in bidirectional hybrid SSMF/FSO using VPI software.

Figure 4 illustrates how the Polarization Beam Splitter (PBS) divides the received AO-OFDM signal initially. It can be seen of as being made up of two perfect linear

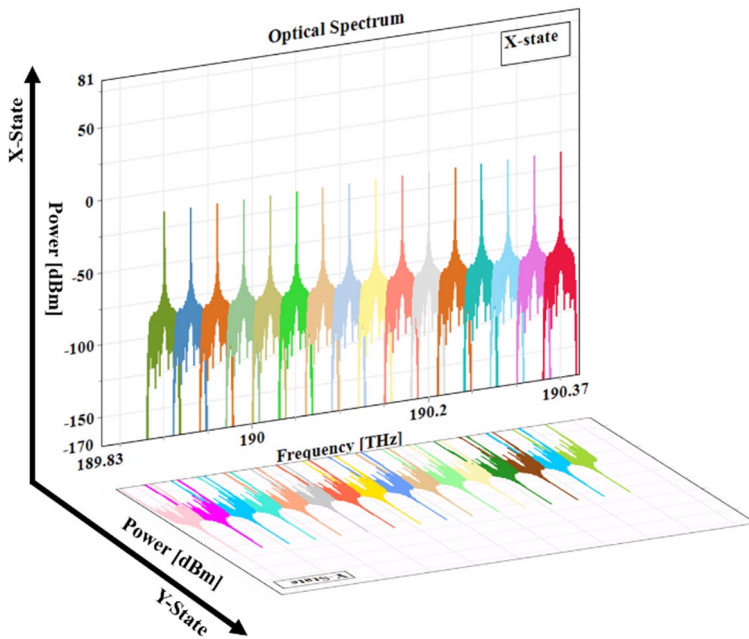


Fig. 4 Polarization Beam Splitter (PBS) operation

polarizers that are placed opposite one another. The ports Output-X and Output-Y output the polarization components of the incoming optical signal that correspond to the device's x- and y-axes (Abd El-Mottaleb et al. 2022; Elsayed et al. 2018; Elsayed and Yousif 2022a, b, c). Following this, an optical demultiplexer divided the X and Y directions, which were then concurrently applied to the direct detection technique (DD). The DFB laser's wavelength and output power are both inside the O-band and are positioned upstream at 1301 nm and 5 dBm, respectively. The DD approach identifies the upstream signal.

4 Results and disussions

The simulation results are shown and discussed in this section. The optical spectrum of a CW laser employed with the OFG source is displayed in Fig. 5a. The study examines the impact of FM frequency deviation on the quantity of OMCs produced. The range of the frequency variation is 10–20 GHz. The spectrum of generated OMCs with a frequency variation of 10 GHz is displayed in Fig. 5b. As can be observed, only 11 optical carriers that have a 30 GHz frequency spacing are able to be produced. According to Fig. 5c, there are 13 optical carriers when the frequency deviation is raised to 15 GHz. Moreover, the number of optical carriers increases to 15 when the frequency deviation is increased to 20 GHz as cleared from Fig. 5d.

Figure 6 shows the relationship between the FM's frequency deviation and the optical carriers that generates at the output. It is noticed that increasing the frequency deviation of the FM from 10 to 60 GHz increases the number of optical carriers. Because, in

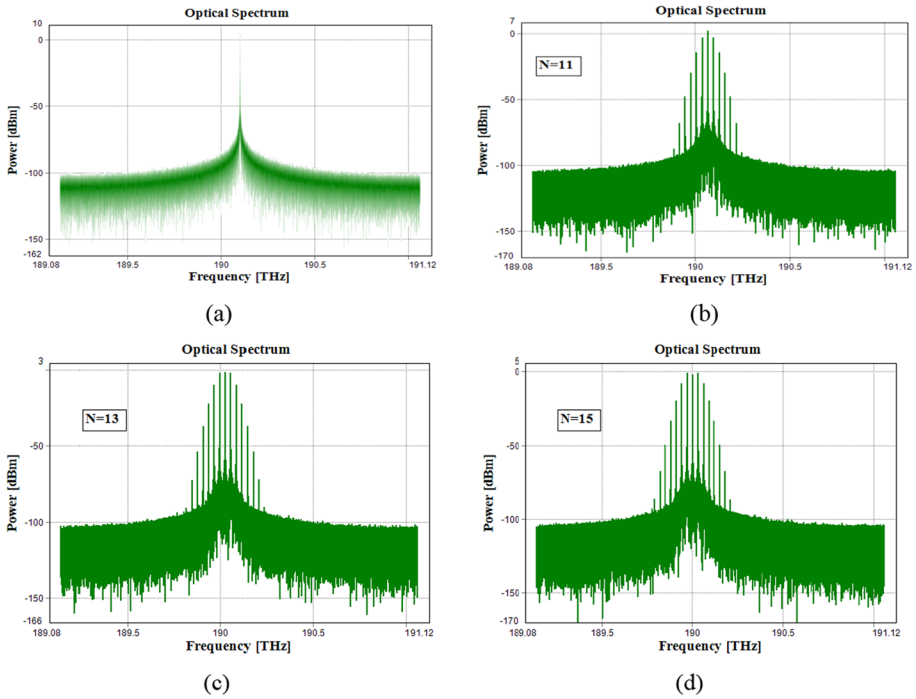


Fig. 5 Optical spectrum of the **a** CW laser source, **b** OMCs by FM 1 at $\Delta f_s = 30$ GHz for different values of the frequency deviation 10 GHz, **c** 15 GHz, and **d** 20 GHz

accordance with Eq. (14), the frequency deviation of FM is correlated with the modulation index of FM (Gao et al. 2016).

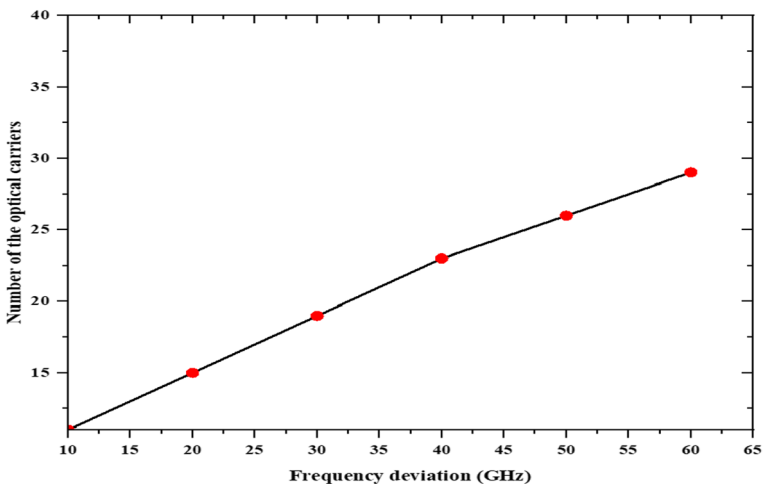


Fig. 6 Relation between the number of OMCs and the frequency deviation of FM $\Delta \nu$

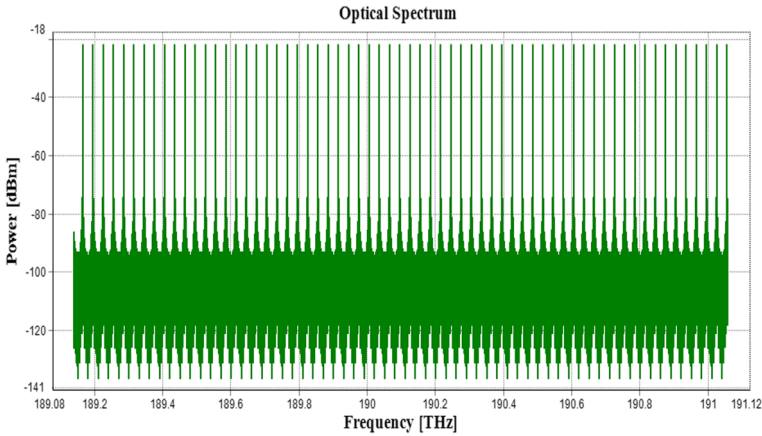


Fig. 7 Optical spectrum of the generated OMCs from cascaded FMs-EAM OFG source with frequency spacing $\Delta f_0 = 30$ GHz

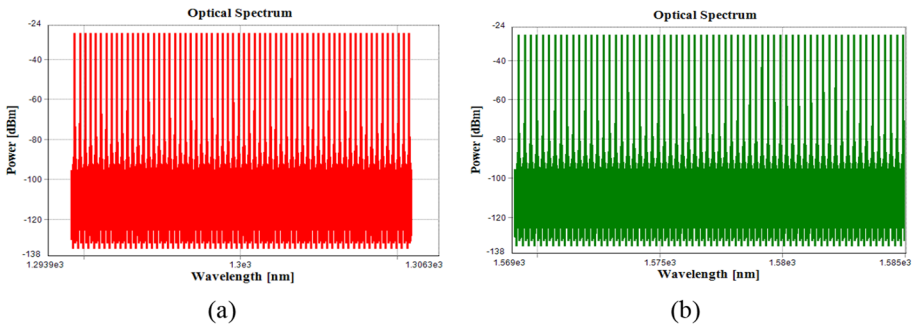


Fig. 8 Optical spectra of the generated optical carriers from cascaded FMs-EAM OFG source with tunable center wavelength **a** $\lambda_c = 1300$ nm corresponds to 230.6 THz and **b** $\lambda_c = 1577$ nm corresponds to 190.1 THz

$$n_{fm} = \frac{\Delta v}{f_0} \tag{14}$$

where, n_{fm} is the modulation index of FM, Δv is the frequency deviation of FM, and f_0 is the frequency of RF signal.

To investigate the capabilities of the suggested cascaded FMs-EAM OFG source, Fig. 7 shows the generated OMCs at the EAM output. At a frequency spacing of 30 GHz, it is discovered that the total number of created OMCs from the EAM is 64, and these carriers have a spectral flatness less than 1 dB.

Therefore, when additional modulators are coupled, the number of optical carriers is significantly enhanced. In 5G PON with upstream/downstream transmission, the tunability of the frequency spacing for the generated OMCs from the FMs-EAM, OFG source is also examined. The frequency spacing of the generated optical carriers can be adjusted by adjusting the frequency of the RF signal, which will result in a carrier frequency spacing that is equal to the frequency of the RF signal. In order to investigate

the potential of the proposed FMs-EAM OFG source at different wavelengths, the CW laser's center frequency (f_c) or wavelength (λ_c) can be adjusted to modify the OFG's centre frequency or wavelength. Additionally, as illustrated in Fig. 8, this OFG source can work at additional optical communication frequencies (such as the O, C, and L bands) to be used in bidirectional 5G PON.

Second, the average power of the CW laser, the length of the SSMF, the FSO range, the BER, the eye diagrams, and the ROP are used to assess the performance of the suggested 5G PON that uses AO-OFDM integrated SSMF/FSO for downstream and upstream transmission. Six subsections comprise the simulation findings. In the first subsection, the impact of difference average power on 5G PON performance is discussed. The performance of the suggested 5G PON using OMCs at different SSMF lengths is studied in the second subsection. The FSO range is varied under various atmospheric turbulences in the third. The impact of air turbulences on the received information signal performance at constant FSO range of 2 km and different is demonstrated in the fourth part. The fifth part examines the impact of varying FSO lengths on the proposed model's performance at a constant SSMF length of 20 km. Lastly, the performance of the suggested model when the position of the ONU is changed is displayed in the last subsection.

4.1 Effect of average power on the performance of the proposed 5G PON

The performance of the suggested 5G PON is impacted by the power of the OFG source. The BER is thus obtained at different values of average powers. Figure 9 shows the BER for 5G PON as a function of average power, with an average power variation of 0–5 dBm. Figure 9a displays the BER performance for the proposed 5G PON in the absence of an optical wireless unit (OWU). It is evident that when average power rises, the BER decreases. The BER values for 5G PON-based AO-OFDM in the presence of OWU, where the signal is transmitted over a range of 2 km, are displayed in Fig. 9b. Similarly, the BER decreases when the CW laser's average power increases. Moreover, it is noted that for reference frequency (190.11 THz), the BER of X-direction is the same as the BER of Y-direction for varying average power of optical source at 20 km (SSMF) and 2 km (FSO link).

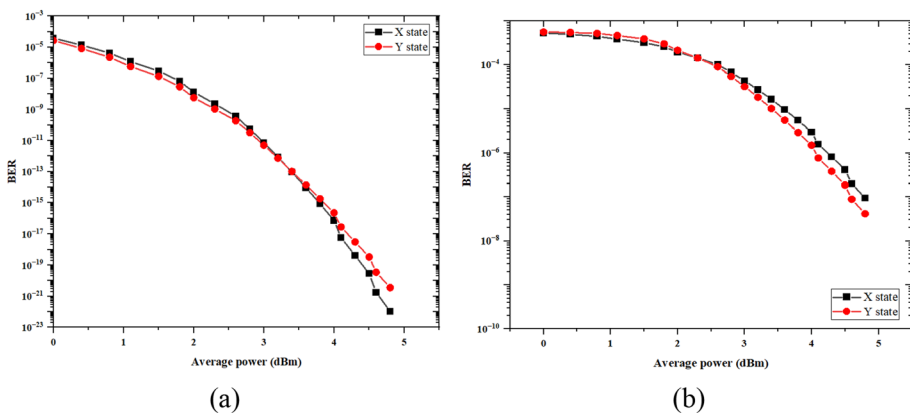


Fig. 9 BER versus average power for 5G PON with **a** SSMF at 20 km and **b** FSO link at 2 km

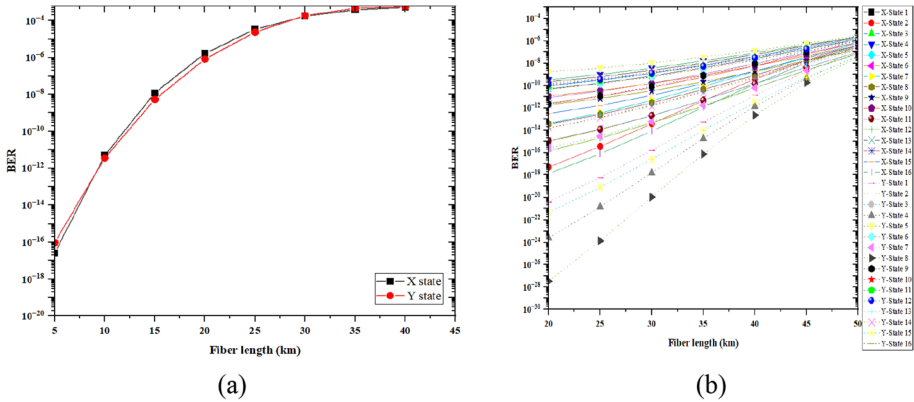


Fig. 10 BER for 5G PON-based SSMF versus different SSMF lengths for **a** the reference channel from 64 channels and **b** 32 channels transmitted through X and Y directions at the ONU side

4.2 Effect of different SSMF lengths on the performance of the proposed 5G PON

In this part, the impact of the SSMF cable length on the suggested 5G PON-based AO-OFDM transmission’s performance is investigated. The BER against variation of fiber length for the channel operating at 190.11 THz is depicted in Fig. 10a. A shorter SSMF length performs better than a longer SSMF length in the X and Y directions. Every transmission distance uses the maximum amount of OMC power (5 dBm), and BER is recorded. For both the X and Y states, the BER increases linearly with increasing transmission distance. This is a result of both fiber nonlinearity and receiver noise. Measuring the maximum transmission distance at the threshold BER ($BER = 1 \times 10^{-9}$) will reveal this. Applying 64 OMCs to the 5G PON yields results of 15 km, while utilizing 32 OMCs yields results of 30 km. These are considered at BER below threshold value (10^{-9}). Furthermore, it is noticed from Fig. 10b that the 5G PON that uses 32 OMCs

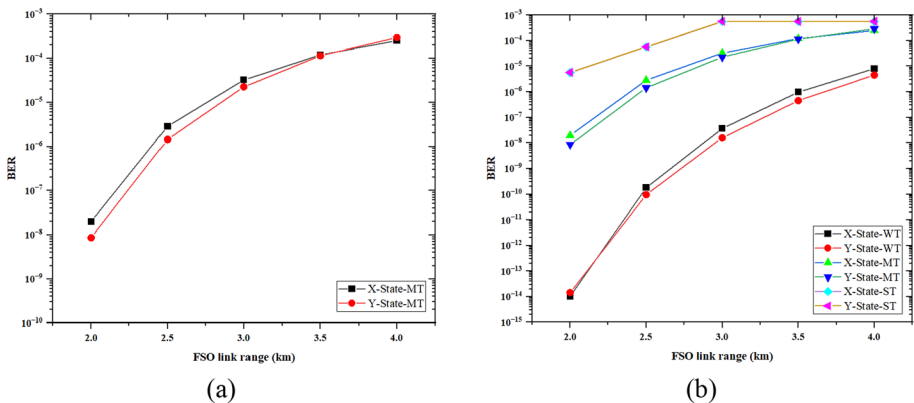


Fig. 11 BER for 5G PON-based FSO versus different FSO ranges for **a** the reference channel from 64 channels under MT and **b** the reference channel from 32 channels transmitted through X and Y directions under WT, MT, and ST at the ONU side

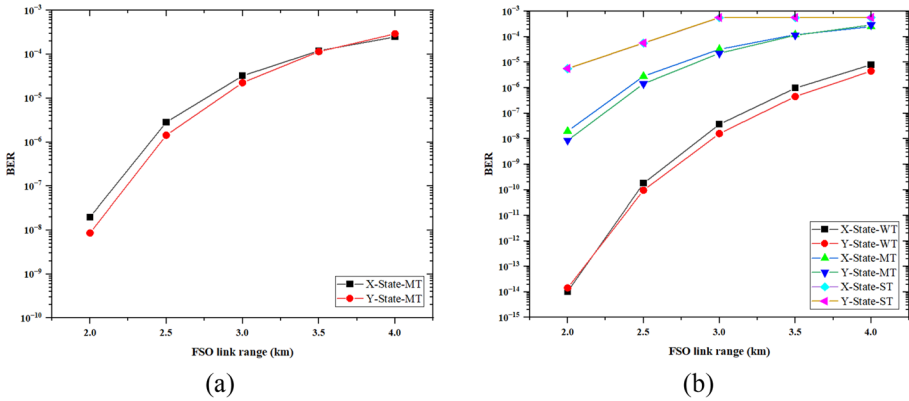


Fig. 12 BER for 5G PON-based FSO versus different FSO ranges for three channels (1, 8, and 16) from 32 channels at a X-direction and b Y-direction under WT, MT, and ST at the ONU side

has a superior BER than the one that uses 64 OMCs. This is because as the number of OMCs increases, the phase noise of the optical carriers also increases.

4.3 Effect of different FSO range on the performance of the proposed 5G PON

Temperature fluctuations result in atmospheric turbulence, which impairs the information signal’s performance as it travels across the FSO channel. Accordingly, this part discussed the impact of different turbulences effects for the suggested model at various FSO ranges. Figure 11a shows the measured BER for the reference channel that transmitted on X and Y states, and Fig. 11b shows the BER for the reference channel from 32 channels with both directions under WT, MT, and ST. Figure 12 shows how WT, MT, and ST affect the BER and various FSO performance of the proposed 5G PON based FSO.

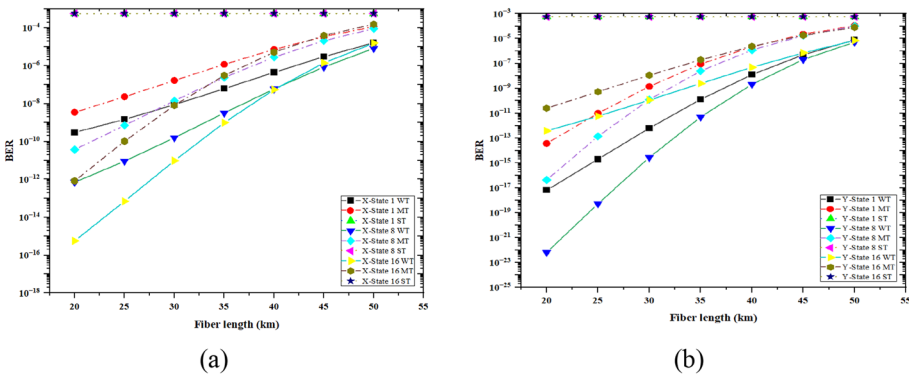


Fig. 13 BER for 5G PON-based SSMF/FSO versus different SSMF lengths for (1, 8 and 16) channels from 32 channels at a X-direction and b Y-direction under WT, MT, and ST at fixed FSO range

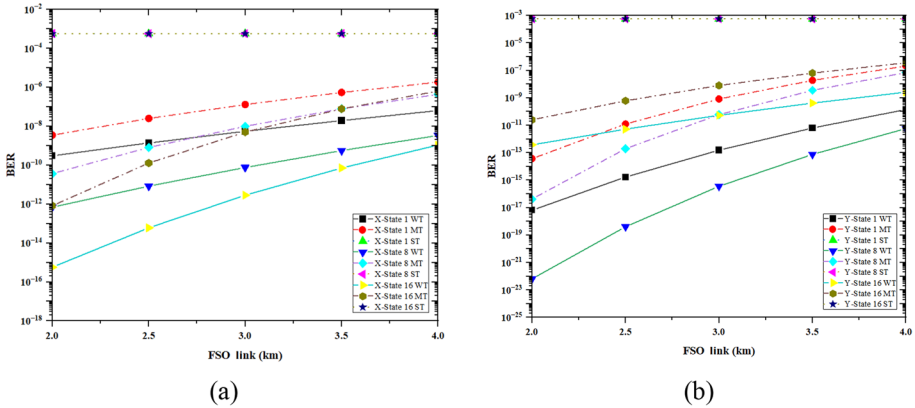


Fig. 14 BER for 5G PON-based SSMF/FSO versus different FSO ranges for (1, 8 and 16) channels from 32 channels at **a** X-direction and **b** Y-direction under WT, MT, and ST at fixed SSMF lengths

4.4 Performance of the proposed 5G PON for varying SSMF length at constant FSO range

The performance of the suggested 5G PON under fixed FSO range of 2 km under WT, MT, and ST and various SSMF distances is given in this part. Figure 13 displays the BER for the channels 1, 8, and 16 at varying fiber lengths for both the X- and Y-states under WT, MT, and ST.

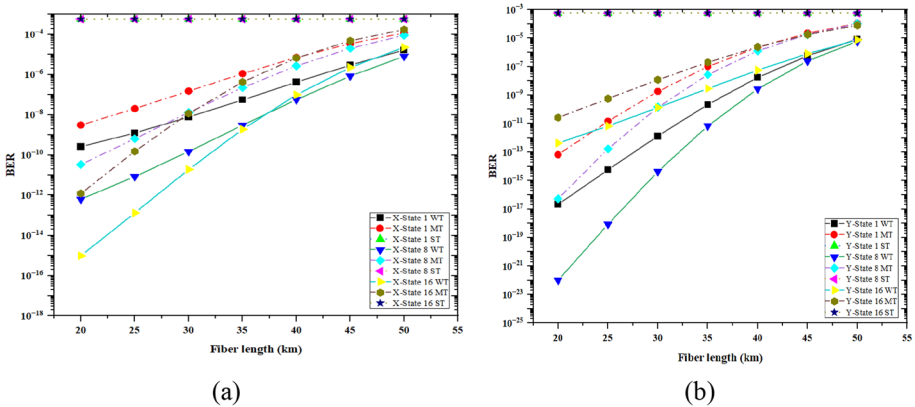


Fig. 15 BER for 5G PON-based SSMF/FSO versus different SSMF lengths for (1, 8 and 16) channels from 32 channels at **a** X-direction and **b** Y-direction under WT, MT, and ST at fixed FSO range with different locations of ONUs

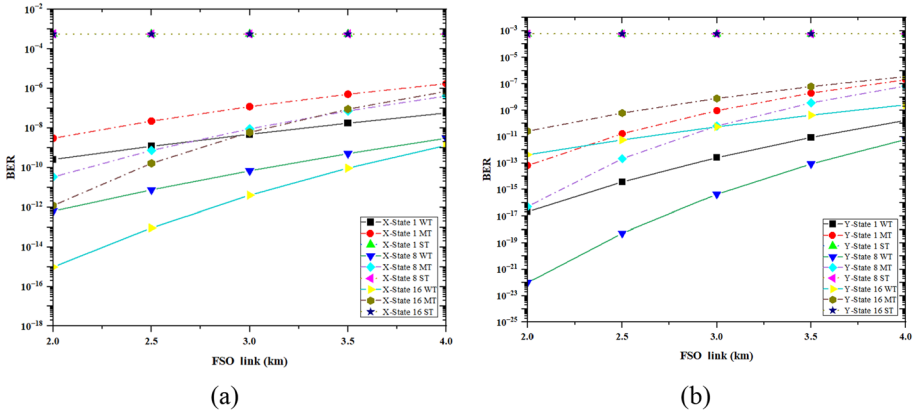


Fig. 16 BER for 5G PON-based SSMF/FSO versus different FSO ranges for (1, 8 and 16) channels from 32 channels at **a** X-direction and **b** Y-direction under WT, MT, and ST at fixed SSMF length with different locations of ONUs

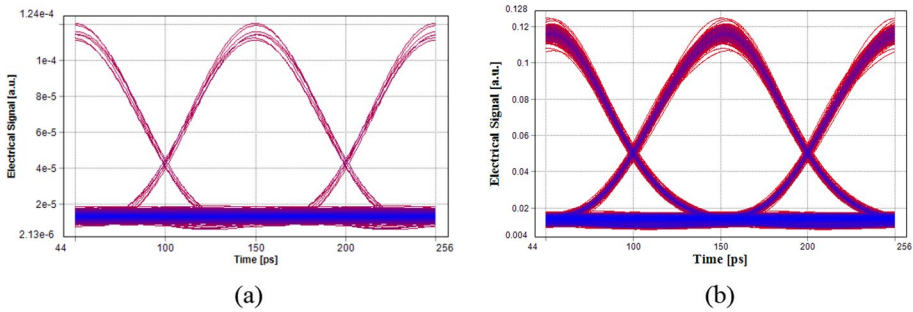


Fig. 17 Eye diagram of the upstream for 5G-PON-based SSMF/FSO under **a** WT and **b** ST

4.5 Performance of the proposed PON for varying FSO range at constant SSMF length

In this part, the performance of the proposed 5G PON based SSMF/FSO at fixed SSMF of 20 km while the FSO ranges are varied. Figure 14 shows the impact of WT, MT, and ST on the BER at various FSO ranges for suggested 5G-PON based SSMF/FSO transmission. All the channels that transmitted on either the X-state or the Y-state reached a propagation range of 4 km with BER $\sim 10^{-4}$. However, when WT is present, the suggested model performs better for all channels, as at the FSO range of 4 km, the BER decrease to 10^{-6} . Since the BER acceptance limit is less than 10^{-3} , all information sent over the 32 channels (960 Gbps) is successfully received.

4.6 Effect of ONU located in different sites for 5G-PON cascaded SSMF/FSO

The variable SSMF from 20 to 50 km, as well as the fixed FSO of 2 km, are taken into consideration in this subsection. Here, the ONUs is dispersed over several locations. For

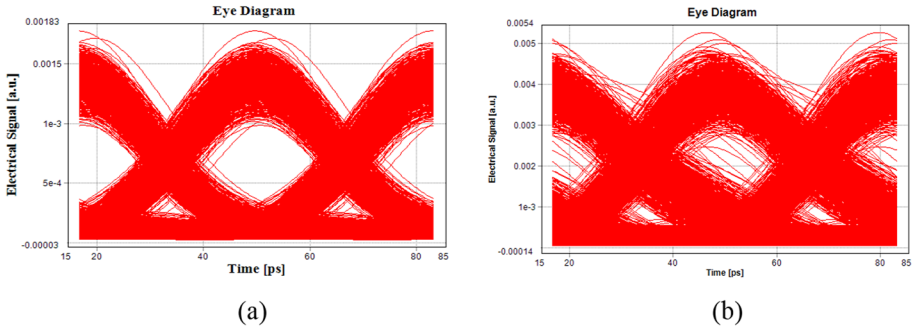


Fig. 18 Eye diagram of the downstream for 5G-PON-based SSMF/FSO under **a** WT and **b** ST

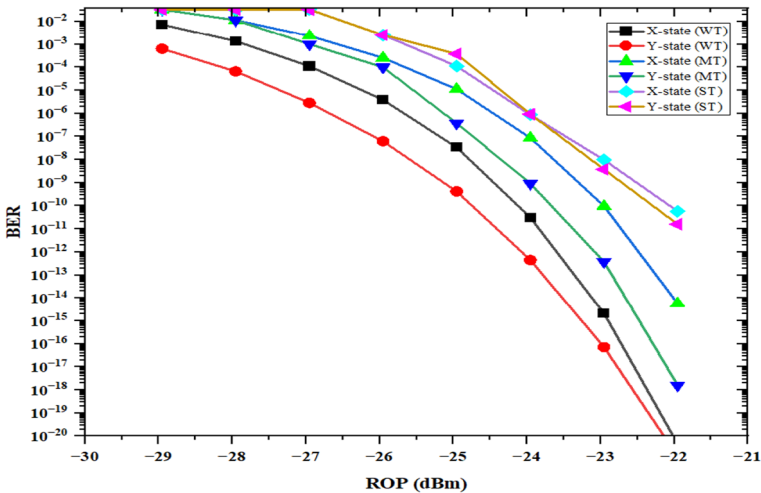


Fig. 19 BER for 5G PON-based SSMF/FSO versus ROP at the reference channel under WT, MT, and ST

the suggested model vs SSMF lengths, Fig. 15a shows the measured BER for channels 1, 8, and 16 that transmitted on the X-state signal, and Fig. 15b shows the BER for the same users who transmitted on the Y-state. One can observe that the BER results in Fig. 15 are almost the same as the BER findings in Fig. 13. As a result, the suggested approach can be applied to mobile communication to send information signals to various locations in a downstream direction. All the channels that transmitted on either the X-state or the Y-state reached a propagation range of 20 km with BER $\sim 10^{-4}$ when the turbulence effects are considered. All of the information data transmitted by the 32 channels (960 Gbps) is successfully received in the downstream direction since the BER's acceptance limit is $<10^{-9}$.

The relationship between the FSO range and the BER performance of (1, 8, and 16) channels when the ONUs is located in various sites under WT, MT, and ST is depicted in Fig. 16. A shorter FSO range provides greater performance than a longer FSO range for all channels. For example, channel 16 transmitted on the X direction under WT has BER equal to 10^{-15} at an FSO range of 2 km, but when the range of the FSO is extended to 4 km, as illustrated in Fig. 16a, this value moves to 10^{-10} . Furthermore, channel 8 transmitted

on Y-direction under WT has BER equal to 10^{-22} if the FSO range is equal to 2 km; when the FSO range exceeds 4 km, as shown in Fig. 16b, this value decreases to 10^{-14} . The eye diagram of the upstream 5G-PON based SSMF/FSO signals, obtained at 20 km (SSMF length)/2 km (FSO range) under WT, is displayed in Fig. 17a. Figure 17b illustrates the eyes opening under the effect of ST. As expected, the opening of the eye becomes small, indicating that the BER performance is deteriorating. While Fig. 18 shows the eye diagram for the downstream direction in the presence of WT (Fig. 18a) and ST (Fig. 18b).

Our results showed that the reported power sensitivity of the selected reference channel is -24.5 dBm at BER 10^{-9} . In the proposed 5G-PON, the forward error correction (FEC) target (BER $< 10^{-3}$) can be used to enable a greater power budget for the hybrid SSMF/FSO link. As a result, as shown in Fig. 19, the obtained power sensitivities are -28 dBm, -26 dBm, and -25 dBm for WT, MT, and ST, respectively.

Furthermore, the resulting FSO sensitivity will decrease as one approaches significant turbulence, as illustrated in Fig. 19. The influences of the atmosphere are what lead to the larger power penalty. Here, the longest FSO traffic length in the 5G PON-based AO-OFDM could be predicted using the measured power budget of certain 5G PON based SSMF/FSO channels, considering the practical requirements of various FSO transmission lengths. Furthermore, in the suggested 5G PON architecture, the appropriate channels can be used to achieve higher FSO sensitivity.

Finally, utilizing the suggested 5G PON, the impact of the pointing error is additionally evaluated under various turbulence conditions. The pointing loss factors (L_t and L_r) of the transmitter and receiver can be determined by (Shrouk M. Moustafa et al. 2021).

$$L_t = e^{(-G_r(\theta_t))^2} \tag{15}$$

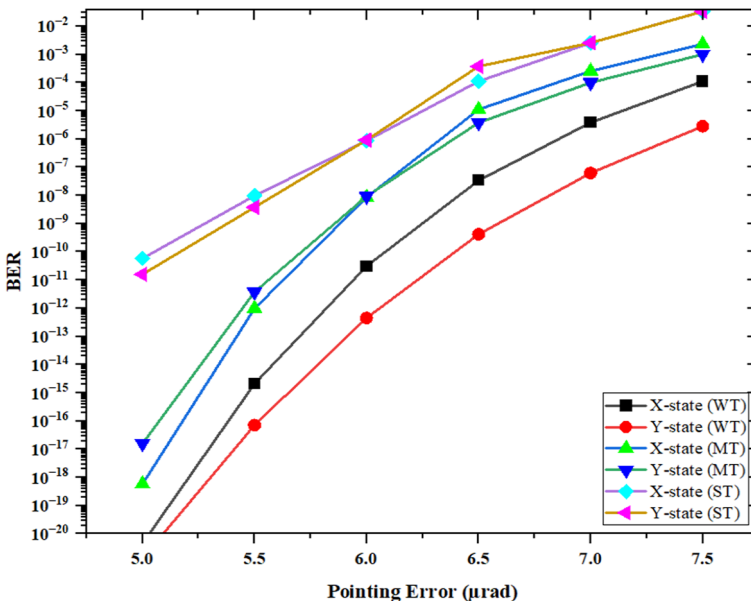


Fig. 20 BER versus pointing error in 5G PON, at different turbulence conditions

Table 3 Comparison between present work and previously published works

References	Technique	Channel	Turbulence effect	Overall capacity (Gbps)
Singh et al. (2021)	MDM	SMF and FSO	Not considered	40
Fady El-Nahal et al. (2022)	Bidirectional WDM-PON	FSO only	WT and ST	320
Fady El-Nahal et al. (2023)	Bidirectional WDM-PON	SMF and FSO	WT and ST	320
Abd El-Mottaleb et al. (2023)	PDM with MDM	MMF and FSO	WT and ST	80
Luay and Mansour (2023)	Comb WDM-PON	SMF	Not considered	140
Present work	AO-OFDM-PON	SMF and FSO	WT, MT, and ST	960

$$L_r = e^{(-G_r(\theta_r)^2)} \quad (16)$$

where θ_t and θ_r are, respectively, the transmitter and receiver pointing error angles. In the FSO link, the power budget is given by (Moustafa et al. 2021).

$$P_{rx} = P_{tx} - \alpha_{sys} - \alpha_{atm} \quad (17)$$

where α_{sys} is system attenuation and α_{atm} is total atmospheric attenuation. In order to give the best signal power received in the FSO channel at a link distance of 2 km, Fig. 20 illustrates the relationship between the BER and the pointing error in the proposed 5G PON. As can be in Fig. 20 that the BER rapidly increases for conditions (WT, MT, and ST) as the pointing error increases. From our results show that, at different values of pointing error under different turbulence, WT gives the optimum BER value.

A comparison between recent published works and present work is shown in Table 3.

5 Conclusion

A novel method for creating OFG using EAM and a cascade of two FMs has been presented in this paper. Each of these modulators is driven by the same RF frequency, with a phase shift of 90 degrees, subsequent to each other. The proposed OFG source's exhibited optical spectrum yielded a generated multicarrier with good spectral flatness (< 1 dB). All 64 of the optical carriers that are produced from the FMs-EAM OFG source fall within a 1 dB spectral flatness. For 5G-PON, the suggested OFG source exhibits good frequency tunability for use in both downstream and upstream transmission directions. The suggested OFG source can increase the capacity of multichannel optical communication systems because of the large number of OMCs it generates. For a high-speed transmission capacity network, an AO-OFDM integrated SSMF/FSO access network based on 5G-PON is suggested. OMCs are generated by the OFG source. Thus, the OFG source produced AO-OFDM signals. The generated OMCs are stable enough and had little dispersion to move in cascaded SSMF/FSO. There are 32 channels allotted to the planned network, with 30 Gbps and 10 Gbps of data available in the downstream and upstream directions, respectively. We investigate two polarization states: X-state and Y-state. To increase 5G PON's capacity, each polarization state carries 30 Gbps. Three different turbulence conditions; WT, MT, and ST, are used when investigating

the proposed 5G-PON performance. Furthermore, a simulation of the 5G PON-based AO-OFDM is conducted to examine the impact of various propagation ranges, average power, and ONU placement. 32 channels can reliably transmit data over propagation ranges of 22 km (20 km SSMF cable + 2 km FSO connection) in the presence of WT with BER less than 10^{-9} , according to the simulation results that are obtained. For the same propagation ranges, these channels can transmit data when the ST presents with BER less than 10^{-3} . Finally, the overall capacity of the proposed 5G PON can reach about 960 Gbps/10 Gbps for downstream/upstream direction. Consequently, our proposed PON model is suggested to be employed in high transmission hybrid wired/wireless networks as well as in PON stage 3 applications of the next generation, such as the 5G communication system. To account for real-time losses and intermodal crosstalk, our model must be experimentally proven. Additionally, we propose to combine alternative multiplexing techniques, such as OCDMA, with the proposed model to increase transmission capacity. Moreover, for just to consider real weather conditions for Baghdad and Alexandria cities.

Authors' contributions IL, TSM, and SAA, have directly participated in the planning, execution, and analysis of this study. All authors have read and approved the final version of the manuscript.

Funding The authors did not receive any funds to support this research.

Declarations

Conflict of interest The authors declare that they have no competing interests.

Availability of data and materials The data used and/or analyzed during the current study are available from the corresponding author on reasonable request.

Ethical approval Not Applicable.

References

- Abd El-Mottaleb, S.A., Métwalli, A., ElDallal, T.A., Hassib, M., Fayed, H.A., Aly, M.H.: Performance evaluation of PDM/SAC-OCDMA-FSO communication system using DPS code under fog, dust and rain. *Opt. Quant. Electron.* **54**, 750 (2022)
- Abd El-Mottaleb, S.A., Singh, M., Ahmed, H.Y., Zeghid, M., Nisar, K.S.: Performance analysis of a spectral-efficient high-speed hybrid PDM-MDM enabled integrated MMF-FSO transmission. *IEEE Photon. J.* **15**(4) (2023)
- Ahmed, H., Soltanian, M.R.K., Amiri, I.S., Alavi, S.E., Othman, A.R., Supa at, A.S.M.: Carriers generated by mode-locked laser to increase serviceable channels in radio over free space optical systems. *IEEE Photon. J.* **7**(5) (2015)
- Andrews, J.G., et al.: What will 5G be? *IEEE J. Sel. Areas Commun.* **32**, 1065–1082 (2014)
- Boccardi, F., Heath, R.W., Lozano, A., Marzetta, T.L., Popovski, P.: Five disruptive technology directions for 5G. *IEEE Commun. Mag.* **52**, 74–80 (2014)
- Chang, G.-k., Liu, C.: 1–100 GHz microwave photonics link technologies for next-generation WiFi and 5G wireless communications in microwave photonics (MWP). In: International Topical Meeting on, pp. 5–8. IEEE. <https://doi.org/10.1109/MWP.2013.6724005> (2013)
- Chaudhary, S., Sharma, A., Tang, X., Wei, X., Sood, P.: A cost effective 100 Gbps FSO system under the impact of fog by incorporating OCDMA-PDM scheme. *Wirel. Pers. Commun.* **116**, 2159–2168 (2020)
- El-Mottaleb, S., Singh, M., Chehri, A., Ahmed, H., Zeghid, M., Khan, A.: Capacity enhancement for free space optics, transmission system using orbital angular momentum optical code division multiple access in 5G and beyond networks. *Energies* **15**(19), 7100 (2022)
- El-Nahal, F., et al.: A bidirectional wavelength division multiplexed (WDM) free space optical communication (FSO) system for deployment in data center networks (DCNs). *Sensors* **22**, 9703 (2022)

- El-Nahal, F., et al.: A bidirectional WDM-PON free space optical (FSO) system for fronthaul 5 G C-RAN networks. *IEEE Photon. J.* **15**, 1 (2023)
- Elsayed, E.E., Yousif, B.B.: Performance enhancement of M-ary pulse-position modulation for a wavelength division multiplexing free-space optical systems impaired by interchannel crosstalk, pointing error, and ASE noise. *Opt. Commun.* **475**, 126219 (2020a)
- Elsayed, E.E., Yousif, B.B.: Performance enhancement of the average spectral efficiency using an aperture averaging and spatial-coherence diversity based on the modified-PPM modulation for MISO FSO links. *Opt. Commun.* **463**, 12546 (2020b)
- Elsayed, E.E., Yousif, B.B.: Performance enhancement of hybrid diversity for M-ary modified pulse-position modulation and spatial modulation of MIMO-FSO systems under the atmospheric turbulence effects with geometric spreading. *Opt. Quant. Electron.* **52**, 508 (2020c)
- Elsayed, E.E., Yousif, B.B.: Performance evaluation and enhancement of the modified OOK based IM/DD techniques for hybrid fiber/FSO communication over WDM-PON systems. *Opt. Quant. Electron.* **52**, 385 (2020d)
- Elsayed, E.E., Yousif, B.B., Alzalabani, M.M.: Performance enhancement of the power penalty in DWDM FSO communication using DPPM and OOK modulation. *Opt. Quant. Electron.* **50**, 282 (2018)
- Elsayed, E.E., Alharbi, A.G., Singh, M., et al.: Investigations on wavelength-division multiplexed fibre/FSO PON system employing DPPM scheme. *Opt. Quant. Electron.* **54**, 358 (2022a)
- Elsayed, E.E., Kakati, D., Singh, M., et al.: Design and analysis of a dense wavelength-division multiplexed integrated PON-FSO system using modified OOK/DPPM modulation schemes over atmospheric turbulences. *Opt. Quant. Electron.* **54**, 768 (2022b)
- Elsayed, E.E., Yousif, B.B., Singh, M.: Performance enhancement of hybrid fiber wavelength division multiplexing passive optical network FSO systems using M-ary DPPM techniques under interchannel crosstalk and atmospheric turbulence. *Opt. Quant. Electron.* **54**, 116 (2022c)
- Fadzlina, N.N., et al.: Design of L-band multiwavelength laser for TDM/WDM PON application in Baghdad. *Sci J* **18**, 4 (2021)
- Feng, J., Zhao, X.: Performance analysis of ook-based fso systems in gamma-gamma turbulence with imprecise channel models. *Opt. Commun.* **402**, 340–348 (2017a)
- Feng, J., Zhao, X.: Performance analysis of ook-based fso systems in gamma-gamma turbulence with imprecise channel models. *Opt. Commun.* **402**, 340–348 (2017b)
- Gao, D., Li, P.-L., Shao, Q., Chen, J.-Y.: Generation of ultra-wide and flat optical frequency comb based on electro-absorption modulator and frequency modulator. *Optoelectron. Lett.* **12**, 97–100 (2016)
- Hammadi, Y.I., Mansour, T.S.: Performance evaluation of all-optical OFDM system-based optical frequency comb source. *J. Mech. Cont. Math. Sci.* **14**, 141–157 (2019)
- Hammadi, Y.I., Hmood, J.K., Mansour, T.S., Harun, S.W.: A tunable optical frequency comb source using cascaded frequency modulator and Mach-Zehnder modulators. *J. Opt. Commun.* **20**(4), 2022–2113 (2022)
- Hamza, A.S., Deogun, J.S., Alexander, D.R.: Classification framework for free space optical communication links and systems. *IEEE Commun. Surv. Tuts.* **21**(2), 1346–1382 (2019)
- Jaffer, S.S., Hussain, A., Qureshi, M.A., Mirza, J., Qureshi, K.K.: A low cost PON-FSO based fronthaul solution for 5G CRAN architecture. *Opt. Fiber Technol.* **63** (2021)
- Jarangal, E., Dhawan, D., Kohli, K., Kaur, R.: Performance enhancement of FSO system under the effect of Scintillation using CWDM. In: *Agrivoltaics2021 Conference: Connecting Agrivoltaics Worldwide* (2022)
- Johansson, L.A., Barton, J.S., Coldren, L.A., Fish, G.A.: High-speed optical frequency modulation in a monolithically integrated widely tunable laser-phase modulator. In: *Optical Fiber Communication Conference, 2004. OFC 2004* (2004)
- Kantarci, B., Moustah, H.T.: Bandwidth distribution solutions for performance enhancement in long-reach passive optical networks. *IEEE Commun. Surv. Tutor.* **14**, 714–733 (2012)
- Kaushal, H., Jain, V., and Kar, S.: Free-space optical channel models. In: *Free Space Optical Communication. Optical Networks*, pp. 41–89. Springer, New Delhi (2017)
- Li, L., Sharma, A.: High speed rgb-based duobinary encoded visible light communication system under the impact of turbulences. *Front. Phys.* **10**, 944623 (2022)
- Li, L., Gu, R., Ji, Y., Bai, L., Huang, Z.: All-optical OFDM network coding scheme for all-optical virtual private communication in PON. *Opt. Fiber Technol.* **10**, 61–67 (2014)
- Li, C.-Y., et al.: A flexible two-way PM-based fiber-FSO convergence system. *IEEE Photon. J.* **10**(2), 1–9 (2018)
- Li, G., Lin, Z., Huang, X., Li, J.: A radio over fiber system with simultaneous wireless multi-mode operation based on a multi-wavelength optical comb and pulse-shaped 4QAM-OFDM. *Electronics* **8**, 1064 (2019). <https://doi.org/10.3390/electronics8101064>

- Luay, I., Mansour, T.S.: Performance investigation for the WDM-passive optical network using multicarrier source. *J. Opt. Commun.* **44**(3), 2022–2113 (2023)
- Luong, D.A., Thang, T.C., Pham, A.T.: Effect of avalanche photodiode and thermal noises on the performance of binary phase-shift keying-subcarrier-intensity modulation/free-space optical systems over turbulence channels. *IET Commun.* **7**, 738–744 (2013)
- Martín-Mateos, P., Porro, A., Acedo, P.: Fully adaptable electro-optic dual-comb generation. *IEEE Photon. Technol. Lett.* **30**, 161–164 (2017)
- Mirza, J., Ghafoor, S., Hussain, A.: A full duplex ultrawideband over free-space optics architecture based on polarization multiplexing and wavelength reuse. *Microw. Opt. Technol. Lett.* **62**, 3999–4006 (2020a)
- Mirza, J., Intiaz, W.A., Aljohani, A.J., Atieh, A., Ghafoor, S.: Design and analysis of a 32× 5 Gbps passive optical network employing FSO based protection at the distribution level. *Alexandria Eng. J.* **59**(6), 4621–4631 (2020b)
- Mirza, J., Ghafoor, S., Hussain, A.: All-optical generation and transmission of multiple ultrawideband signals over free space optical link. *Opt. Eng.* **58**(5) (2019)
- Mori, K., Takara, H., Kawanishi, S.: Analysis and design of supercontinuum pulse generation in a single-mode optical fiber. *J. Opt. Soc. Amer. B* **18**(12), 1780–1792 (2001)
- Moustafa, S.M., Fayed, H.A., Aly, M.H.M.: SISO and MIMO FSO based links under different weather conditions: system evaluation. *Opt. Quant. Electron.* **53**, 674 (2021)
- Osseiran, A., et al.: Scenarios for 5G mobile and wireless communications: the vision of the METIS project. *Commun. Mag. IEEE* **52**, 26–35 (2014)
- Sharma, A., Malhotra, J.: Simulative investigation of FMCW based optical photonic radar and its different configurations. *Opt. Quant. Electron.* **54**, 233 (2022)
- Shbair, W.W., El-Nahal, F.I.: Coherent passive optical network for 5G and beyond transport. *Optoelectron. Lett.* **17**(9), 546–551 (2021)
- Singh, M., Aly, M.H., Abd El-Mottaleb, S.A.: Performance analysis of a 448 Gbps PDM/WDM/16-QAM hybrid SMF/FSO system for last mile connectivity. *Opt. Quant. Electron.* **55**, 231 (2023)
- Singh, H., Mittal, N., Miglani, R., Majumdar, A.K.: Mode division multiplexing (mdm) based hybrid PONFSO system for last-mile connectivity. In: 2021 Third South American Colloquium on Visible Light Communications (SACVLC), Toledo, Brazil, 01–06, 11–12 November (2021)
- Ujjwal, Thangaraj, J.: Generation of ultra-wide and flat optical frequency comb based on electro absorption modulator. *Optoelectron. Lett.* **14**(3) (2018)
- Vetelino, F.S., Young, C., Andrews, L., Reclons, J.: Aperture averaging effects on the probability density of irradiance fluctuations in moderate-to-strong turbulence. *Appl. Opt.* **46**, 2099–2108 (2007)
- Yeh, C.-H., Guo, B.-S., Chang, Y.-J., Chow, C.-W., Gu, C.-S.: Bidirectional free space optical communication (FSO) in WDM access network with 1000-m supportable free space link. *Opt. Commun.* **435**, 394–398 (2019)
- Yeh, C.-H., Chen, J.-R., You, W.-Y., Lin, W.-P., Chow, C.-W.: Free space optical communication in long-reach unidirectional ring architecture fiber network. *IEEE Access* **8**, 159574–159580 (2020)
- Yousif, B.B., Elsayed, E.E.: Performance enhancement of an orbital-angular-momentum-multiplexed free-space optical link under atmospheric turbulence effects using spatial-mode multiplexing and hybrid diversity based on adaptive MIMO equalization. *IEEE Access* **7**, 84401–84412 (2019)
- Yousif, B.B., Elsayed, E.E., Alzalabani, M.M.: Atmospheric turbulence mitigation using spatial mode multiplexing and modified pulse position modulation in hybrid RF/FSO orbital-angular-momentum multiplexed based on MIMO wireless communications system. *Optics Commun* **436**, 197–208 (2019)

Publisher's Note Springer Nature remains neutral with regard to jurisdictional claims in published maps and institutional affiliations.

Springer Nature or its licensor (e.g. a society or other partner) holds exclusive rights to this article under a publishing agreement with the author(s) or other rightsholder(s); author self-archiving of the accepted manuscript version of this article is solely governed by the terms of such publishing agreement and applicable law.